

Global MRI with Braginskii viscosity in a galactic profile

M. S. Rosin^{1,2*} and A. J. Mestel³

¹ *UCLA Department of Math, 520 Portola Plaza, Los Angeles, CA 90095, U.S.A.*

² *DAMTP, Centre for Mathematical Sciences, University of Cambridge, Wilberforce Road, Cambridge, CB3 0WA, U.K.*

³ *Department of Mathematics, Imperial College, South Kensington Campus, London, SW7 2AZ, U.K.*

Submitted to MNRAS April 2012

ABSTRACT

We present a global-in-radius linear analysis of the axisymmetric magnetorotational instability (MRI) in a collisional magnetized plasma with Braginskii viscosity. For a galactic angular velocity profile Ω we obtain analytic solutions for three magnetic field orientations: purely azimuthal, purely vertical and slightly pitched (almost azimuthal). In the first two cases the Braginskii viscosity damps otherwise neutrally stable modes, and reduces the growth rate of the MRI respectively. In the final case the Braginskii viscosity makes the MRI up to $2\sqrt{2}$ times faster than its inviscid counterpart, even for *asymptotically small* pitch angles. We investigate the transition between the Lorentz-force-dominated and the Braginskii viscosity-dominated regimes in terms of a parameter $\sim \Omega\nu_B/B^2$ where ν_B is the viscous coefficient and B the Alfvén speed. In the limit where the parameter is small and large respectively we recover the inviscid MRI and the magnetoviscous instability (MVI). We obtain asymptotic expressions for the approach to these limits, and find the Braginskii viscosity can magnify the effects of azimuthal hoop tension (the growth rate becomes complex) by over an order of magnitude. We discuss the relevance of our results to the local approximation, galaxies and other magnetized astrophysical plasmas. Our results should prove useful for benchmarking codes in global geometries.

Key words: instabilities – accretion, accretion discs – Galaxy: disc – MHD – magnetic fields – plasmas.

1 INTRODUCTION

In the formation of compact objects (stars, planets and black holes) from accretion discs, turbulence driven by the MRI, and possibly the MVI, offers a promising mechanism for the necessary angular momentum transport (Velikhov 1959; Chandrasekhar 1960; Balbus & Hawley 1991; Balbus 2004). It has also been suggested that the observed velocity fluctuations $\sim 6 \text{ km s}^{-1}$ in parts of the interstellar medium (ISM) with low star formation rates may, in part, arise from this process (Sellwood & Balbus 1999; Tamburro et al. 2009). The evidence for this comes primarily from numerical simulations and a wide range of studies agree that weak magnetic fields and outwardly decreasing angular velocity profiles are an unstable combination (Balbus & Hawley 1998; Balbus 2003).

The most illuminating explanation for this comes from a shearing sheet analysis in which the mean azimuthal flow of the differentially rotating disc is locally approximated by a constant angular velocity rotation plus a linear velocity shear (Goldreich & Lynden-Bell 1965; Umurhan & Regev

2004). In the simplest possible setup, incompressible, isothermal, dissipationless, axisymmetric linear perturbations to a magnetic field with a weak vertical component, i.e. parallel to the rotation axis of the disc, are unstable when the angular velocity decreases away from the disc’s centre. Azimuthal velocity perturbations to fluid elements at different heights, tethered to each other by the magnetic field, increase (decrease) their angular momentum. This causes them to move to larger (smaller) radii as dictated by the gravitational field which sets the mean flow. In the frame rotating at constant angular velocity, this motion deforms the tethering magnetic field, provided it is not too strong, and this induces a prograde (retrograde) Lorentz force on the outer (inner) element thus destabilising the system as it moves to yet larger (smaller) radii. This mechanism is at the heart of the MRI.

However, although this model and description captures much of the essential physics, to fully understand the MRI, or at least the framework within which the shearing sheet should exist, a more nuanced approach is needed. In part, this is because the shearing sheet is formulated in a Cartesian coordinate system where curvature terms that arise naturally from the cylindrical geometry of the accretion disc

* E-mail: msr35@math.ucla.edu

are neglected. Indeed, in the local approximation, the over-stabilising effects of hoop tension (a curvature effect) associated with the azimuthal magnetic field, are totally ignored. Furthermore, the model predicts that the fastest growing, and therefore most physically relevant, linear MRI modes have a homogeneous radial structure on the scale of the shearing sheet in which the local approximation is made (Guan et al. (2009) has shown the MRI is well localized in the non-linear regime). This means that the global disc structure, including boundary conditions, not captured by the local approximation may have a significant effect on these large scale modes in a way that cannot be determined locally. Other limitations exist too (Knobloch 1992; Regev & Umrhan 2008).

The extent to which these limitations matter should, and under a variety of assumptions have, been investigated by global analyses that take into account the full radial structure of the disc and its boundaries (Dubrulle & Knobloch 1993; Curry et al. 1994; Curry & Pudritz 1995; Ogilvie & Pringle 1996; Ogilvie 1998), and specifically for the galaxy by Kitchatinov & Rüdiger (2004). The conclusions of these investigations largely confirms the local picture of a large radial scale instability driven by the differential rotation of the disc. This suggests that whilst a local MRI analysis is generally correct, its regime of validity must be checked globally. It is the purpose of this work to do just that for the MRI operating in a collisional, *magnetized* (the ion cyclotron frequency $\omega_i \gg$ ion-ion collision frequency ν_{ii}) plasma (like the ISM).

In such a plasma Braginskii (1965) has shown that to lowest order in ω_i/ν_{ii} , the deviatoric stress tensor is diagonal and anisotropic. This leads to different parallel and perpendicular viscosities or, more fundamentally, pressures (and thermal conductivities¹) with respect to the local direction of the magnetic field. Of the important physical consequences of this, it will be the effect of the Braginskii viscosity in the presence of a galactic shear flow that will concern us here.

This is not a new topic and in recent years the study of magnetized accretion discs has attracted attention in both the collisionless (Quataert et al. 2002; Sharma et al. 2003, 2006, 2007) and collisional regimes (Balbus 2004; Islam & Balbus 2005; Ferraro 2007; Devlen & Pekünli 2010), and a well developed code to simulate them now exists (Parrish & Stone 2007; Stone et al. 2008). However, a number of fundamental questions remain unanswered. Primarily, what is the non-linear fate of the MRI in a collisional magnetized plasma? Does it transport angular momentum and if so, is the transporting stress primarily viscous, Maxwell or Reynolds²? On what scales do the most unstable modes emerge and how does this vary with the system parameters? In what regime will a local analysis become untenable

and global effects (either radial or vertical) become important (Gammie & Balbus 1994)? What effect does the presence, or absence, of a net vertical field have given Cowling's anti-dynamo theorem and the dissipative properties of the Braginskii viscosity (Moffatt 1978; Lyutikov 2007)? Could viscous heating from the Braginskii viscosity lead to secondary magnetized or unmagnetized thermal instabilities (Balbus 2001; Quataert 2008; Kunz et al. 2011)? Do channel solutions, or something approaching them, emerge (Goodman & Xu 1994)? If they do, the associated field growth will generate pressure anisotropies that could feed new parasitic instabilities such as the mirror. What would their effects be at this stage and in the inevitable turbulence where the mirror and firehose instabilities will both arise (Schekochihin et al. 2005)?

Addressing these questions will require a two-pronged approach involving both numerical and analytic studies. It may transpire that much of the existing work on the unmagnetized and collisionless MRI is directly applicable, but this needs determining. As such we conduct a global linear stability analysis for three separate background magnetic field orientations: purely azimuthal, purely vertical and pitched (magnetic field lines follow helical paths on cylinders of constant radius). We embed these in a galactic rotation profile. In agreement with earlier, local studies, we find that when the field has both a vertical and an azimuthal component, a linear instability with a real part up to $2\sqrt{2}$ times faster than the MRI emerges (Balbus 2004; Islam & Balbus 2005). In contrast to local studies we also find that it has a travelling wave component, and its growth rate depends on the viscous coefficient.

In the presence of a vertical field, we also recover the standard inviscid MRI and show that upon introducing the Braginskii viscosity, its growth rate is always reduced. A similar effect is found for a purely azimuthal field where we find that the Braginskii viscosity damps modes that are, inviscidly, neutrally stable.

The layout of this paper is as follows. In Section 2, we introduce and perturb a series of equilibrium solutions to the Braginskii-MHD equations and this forms the basis of our global stability analysis. Relegating the manipulation of the perturbed equations to Appendix A, we obtain a single ODE governing the perturbed modes. We proceed by solving this for azimuthal, vertical and pitched field orientations in Sections 3, 4 and 5 respectively. For each case we contrast the behaviour with and without Braginskii viscosity. In Section 6 we discuss the physical mechanism of the instability, where it may occur astrophysically, and the relation of our results to the local approximation. Finally, we conclude in Section 7 with some thoughts on open questions relating to magnetized astrophysical plasmas.

2 GLOBAL STABILITY ANALYSIS

2.1 Governing equations

The simplest set of equations that capture the physics of the collisional magnetized MRI are those of isothermal ideal MHD with the Braginskii viscosity (Lifshitz et al. 1984). Explicitly these equations are the momentum equation, including the Braginskii stress tensor; the induction

¹ In the presence of temperature gradients, anisotropic thermal conduction can lead to the magnetothermal (Balbus 2000) and heat flux buoyancy instabilities (Quataert 2008).

² Simulations in the collisionless regime by Sharma et al. (2006) shows that there is angular momentum transport and the anisotropic pressure constitutes a significant portion of the total stress (\sim Maxwell and \gg Reynolds).

equation that describes the evolution of the magnetic field; the incompressibility condition (because the perturbations are linear, the Mach number can always be made small enough to ensure this); and the stress tensor itself:

$$\frac{\partial \mathbf{u}}{\partial t} + \mathbf{u} \cdot \nabla \mathbf{u} = -\nabla \Pi + \mathbf{B} \cdot \nabla \mathbf{B} - \nabla \Phi_D - \nabla \cdot \mathbf{T}, \quad (1)$$

$$\frac{\partial \mathbf{B}}{\partial t} + \mathbf{u} \cdot \nabla \mathbf{B} = \mathbf{B} \cdot \nabla \mathbf{u}, \quad (2)$$

$$\nabla \cdot \mathbf{u} = 0, \quad (3)$$

$$\mathbf{T} = \nu_B (\mathbf{I} - 3\mathbf{b}\mathbf{b}) \mathbf{b}\mathbf{b} : \nabla \mathbf{u}, \quad (4)$$

where the constant mass density has been scaled out of the problem, \mathbf{u} is the velocity field, \mathbf{B} is the mass-density scaled magnetic field, i.e. the Alfvén velocity, $\mathbf{b} = \mathbf{B}/B$ is the direction of the magnetic field, Φ_D is the gravitational potential, $\Pi = p + B^2/2$ is the total (gas plus magnetic) pressure, ‘ \cdot ’ is the full inner product, \mathbf{I} the identity, and \mathbf{T} is the full Braginskii stress tensor whose form we now explain.

In a magnetized plasma the total pressure tensor $\mathbf{P} = p\mathbf{I} + \mathbf{T}$ (whose divergence appears in the momentum equation) is given by

$$\mathbf{P} = p\mathbf{I} + \frac{1}{3} (\mathbf{I} - 3\mathbf{b}\mathbf{b}) (p_\perp - p_\parallel),$$

where p_\perp, p_\parallel are the perpendicular and parallel scalar pressures with respect to the magnetic field direction. When the plasma is also collisional, the pressure anisotropy $p_\perp - p_\parallel$ can be related to the rate-of-strain by a Chapman-Enskog style perturbation theory (Braginskii 1965; Chapman & Cowling 1970).

Microphysically, the anisotropy arises from the conservation of the magnetic moment (first adiabatic invariant) of a gyrating particle in a magnetic field. However, collisions break this conservation and relax the anisotropy by pitch-angle scattering particles in velocity space (this dissipative process will turn out to be important in isolated field configurations). The competition between these two processes is governed by

$$\frac{d}{dt}(p_\perp - p_\parallel) \simeq 3p \frac{d \ln B}{dt} - \nu_{ii}(p_\perp - p_\parallel),$$

where we have used the BGK operator to approximate the full collision operator.

In the presence of time-varying magnetic fields, the pressure anisotropy tends to a steady state that tracks the fields’ rate of change. It follows

$$p_\perp - p_\parallel = 3\nu_B \frac{d \ln B}{dt} = 3\nu_B \mathbf{b}\mathbf{b} : \nabla \mathbf{u},$$

where $\nu_B \sim p/\nu_{ii}$ is the coefficient of the Braginskii viscosity, and we have used equation (2) in the final equality. Equation (4) follows directly.

2.2 Equilibrium solutions

Working in cylindrical polar coordinates (r, ϕ, z) , we introduce equilibrium solutions to equations (1)-(4) that describe a differentially rotating global shear flow constrained by gravity and threaded by a magnetic field that lies on cylinders of constant radius. Our equilibrium solutions are uniform in z , and the plasma motion is restricted at an inner boundary of finite radius r_0 . (The validity of these assumptions will be discussed in Section 6.2.)

We allow gravity $\nabla \Phi_D$ to dictate the rotation profile of the equilibrium flow $\Omega = \Omega_0(r/r_0)^{-q}$ where Ω_0 is the rotation frequency at the inner boundary and q is a dimensionless measure of the shear. Of interest to us here is the case of $q = 1$ that is both analytically treatable and physically corresponds to a galactic disc where, unlike the Keplerian case of $q = 3/2$, the gravitational potential of the *dark matter halo* sets the rotation profile (Rubin & Ford 1970; Sofue & Rubin 2001). In modelling this we set the dark matter mass distribution (whose sole purpose is to ultimately set the rotation profile) to a Mestel (1963) profile so, via Poisson’s equation, $\nabla \Phi_D \propto 1/r$. In this case, the flow $\mathbf{u} = \Omega(r)r\hat{\mathbf{e}}_\phi = \Omega_0\hat{\mathbf{e}}_\phi$ does not vary with radius.

We decompose the magnetic field into vertical and azimuthal components, (so as to construct a time independent equilibrium, we neglect radial magnetic fields³). That is, $\mathbf{B} = B_z\hat{\mathbf{e}}_z + B_\phi\hat{\mathbf{e}}_\phi = B(\sin\theta\hat{\mathbf{e}}_z + \cos\theta\hat{\mathbf{e}}_\phi)$ where $\theta = \arctan(B_z/B_\phi)$ is the pitch angle of the magnetic field. We do not specify θ yet, however, for mathematical simplicity, we demand that both B_ϕ and B_z are independent of radius so θ remains constant. Whilst this implies a vertical current $\propto 1/r$ is associated with B_ϕ , a simple super-galactic magnetic field can account for B_z . In all, our equilibrium fields take the form

$$\mathbf{u} = \Omega_0\hat{\mathbf{e}}_\phi, \quad \mathbf{B} = B_z\hat{\mathbf{e}}_z + B_\phi\hat{\mathbf{e}}_\phi, \quad (5)$$

and are constant in space and time. As is physically relevant, we restrict $B/\Omega < 1$.

It is a mathematically convenient feature of our equilibrium solutions that there is no evolution of the magnetic field strength. From equations (4) and (5), \mathbf{T} is absent from the unperturbed state and the system will be stable to pressure anisotropy driven microscale instabilities, e.g. firehose and mirror (Schekochihin et al. 2005). In contrast to the case where Laplacian viscosity (or indeed resistivity) is present, we can construct an ideal MHD solution independent of any radial flows (Kersalé et al. 2004).

2.3 Perturbed equations

To determine the stability of this system we linearise equations (1)-(4) about (5) with axisymmetric velocity perturbations $\delta\mathbf{u} = \delta\mathbf{u}(r)\exp[ikz + \gamma t]$ and similarly for the magnetic and pressure fields. Here k is the wavenumber in the z direction and γ the growth rate. We retain curvilinear terms from the cylindrical geometry but neglect self-gravity. We non-dimensionalise with respect to time-scales Ω_0 and length-scales r_0 .

As detailed in Appendix A, the linearised equations combine into a single *complex* second order ordinary differential equation for δu_r , the Modified Bessel equation

$$\frac{d^2 \delta u_r}{dr^2} + \frac{1}{r} \frac{d \delta u_r}{dr} - \left(p^2 - \frac{v^2}{r^2} \right) \delta u_r = 0, \quad (6)$$

³ Although magnetic field configurations vary from galaxy to galaxy, they are commonly found tracing the spiral arms and therefore, in the plane of the disc, predominantly azimuthal. Beck et al. (1996) gives values for the mean in-plane field $B_r/B_\phi \sim 0.25$ thereby justifying, to some degree, our neglect of the radial field.

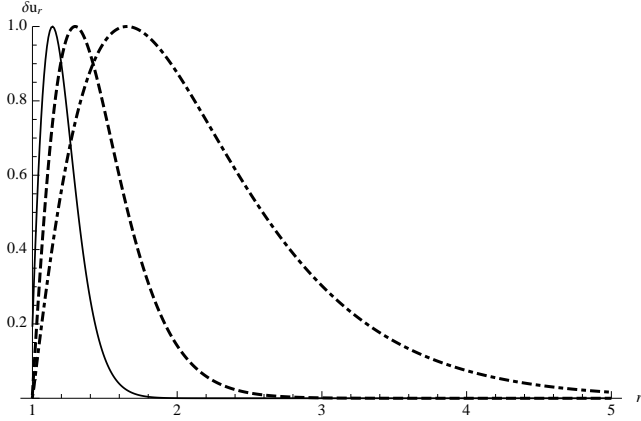


Figure 1. Radial mode structure of the fastest growing $n = 0$ branch MRI modes with $\theta = \pi/2, z = 0, B = 2.0 \cdot 10^{-2}$ and $S_B = 10$ (solid), 10^2 (dashes), 10^3 (dots/dashes). The (purely real) growth rates are $\gamma_m = 0.39, 0.31, 0.19$ and associated wavenumber $k_m = 36.0, 30.0, 20.6$.

where

$$p^2 \equiv \frac{k^2}{E_1} (\sigma^2 + \gamma^2) (\sigma^2 + \gamma^2 + S_B \gamma \sigma^2 \cos^2 \theta), \quad (7)$$

$$v^2 \equiv -\frac{1}{E_1} (\gamma^4 + a_3 \gamma^3 + a_2 \gamma^2 + a_1 \gamma + a_0), \quad (8)$$

and

$$\begin{aligned} E_1 &= (\sigma^2 + \gamma^2) (\sigma^2 + \gamma^2 + S_B \gamma \sigma^2), \\ a_3 &= S_B \sigma^2 [\cos^2 \theta (\cot^2 \theta - 1) + \sin^2 \theta], \\ a_2 &= 2[\sigma^2 (1 + \cot^2 \theta) + k^2] + 2i S_B \sigma^2 \sin 2\theta k (1 - \cot^2 \theta), \\ a_1 &= S_B \sigma^4 [\cos^2 \theta (3 - 2k^2 \sigma^{-2}) + 1 - \cot^2 \theta] - 8i \sigma^2 k \cot \theta, \\ a_0 &= \sigma^2 [\sigma^2 (1 - 2 \cot^2 \theta) - 2k^2]. \end{aligned}$$

Here $\sigma \equiv k B \sin \theta$ is the vertical Alfvén frequency and $S_B = 3\nu_B/B^2$ ($= 3\nu_B \Omega_0/(B^2 n m_i)$ in dimensional form) $\simeq \beta/\nu_{ii}$ is a measure of the relative sizes of the anisotropic pressure force and Lorenz force⁴. Here n is the number density, m_i the ion mass and β the plasma-beta.

To obtain solutions to equation (6), we choose our boundary conditions to be an impenetrable wall at r_0 so $\delta u_r(r_0) = 0$ and the requirement $r^{\frac{1}{2}} \delta u_r$ decays at infinity (see Furukawa et al. (2007) for an inviscid treatment that includes the shear singularity at the origin).

In this case, the eigenfunctions of equation (6) are modified Bessel functions of the second kind $K_{iv}(pr)$ with argument pr and order v (Watson 1944; Abramowitz & Stegun 1964). The spectrum of solutions is discrete and we index v with n, v_n . In the special case when p (or γ from equation (7)) is real (in general it is complex) the problem is Sturm-Liouville and v_n is an infinite ordered set of eigenvalues $v_0 < v_1 < v_2 \dots < v_\infty$. To determine v_n and therefore

⁴ Using a Landau fluid closure and including the effect of collisions Quataert et al. (2002); Sharma et al. (2003) were the first to show the dependence of the MRI on Ω, ν_{ii} and β . Because the closure for the pressure anisotropy differs between the collisionless and Braginskii regimes, the transition between the pressure anisotropy driven MRI, and the MHD MRI scales, in dimensional form, as $(\nu_{ii}/\Omega)\beta^{1/2}$ there, and $(\nu_{ii}/\Omega)\beta$ here.

γ , it is necessary to solve

$$K_{iv_n}(p) = 0. \quad (9)$$

From solutions to this and equations (7) and (8), the full set of flow, magnetic and pressure fields can be constructed, Appendix A. In Fig. 1 we show the radial structure of δu_r when $\theta = \pi/2$.

In general, determining γ must be done numerically. However, for the most physically relevant magnetic field configurations, the problem becomes, in part, analytically tractable. These cases, a purely azimuthal field $\theta = 0$ (in the galactic plane), a purely vertical field $\theta = \pi/2$ (a supergalactic field) and a slightly pitched field $\theta \ll 1$ (very slightly out of the galactic plane), exhibit categorically different behaviour such that $\theta \rightarrow 0, \pi/2$ are singular limits.

In the first case, linear perturbations are damped; in the second, the system is unstable to the MRI but the Braginskii viscosity reduces the maximum growth rate γ_m below the Oort-A value maximum $|d \ln \Omega / d \ln r| = 1/2$, (Balbus & Hawley 1992); in the third, the system is unstable with $\gamma_m \rightarrow \sqrt{|d \ln \Omega^2 / d \ln r|} = \sqrt{2}$, even for *asymptotically small* θ (Balbus 2004). We present the details of these calculations now.

3 AZIMUTHAL FIELD, $\theta = 0$

The stability of inviscid axisymmetric perturbations to a purely azimuthal magnetic field in the presence of a shear flow are well known. When $q < 2$ and the magnetic field $\mathbf{B} = B r^{-d} \hat{\mathbf{e}}_\phi$ has $d > -1$ the system is always stable (as ours is). When only one criterion is met, depending on the form of the fields, the system may still remain stable by the modified Rayleigh criterion (Rayleigh 1916; Michael 1954; Chandrasekhar 1961). (It is worth noting however that global non-axisymmetric perturbations are unstable (Ogilvie & Pringle 1996).)

Do these results for our inviscidly stable system, $\mathcal{R}(\gamma) = 0$, persist in the presence of the Braginskii viscosity? The answer is no.

Setting $\theta = 0$ in equations (6) to (8) and making a change of variables, $\delta u_r \rightarrow r^{-1/2} \delta u_r$, we obtain the simple expression

$$\gamma^2 \frac{d^2 \delta u_r}{dr^2} - (\gamma^2 Q_1 + \gamma Q_2 + Q_3) \delta u_r = 0, \quad (10)$$

where

$$Q_1 = \frac{3}{4} \frac{1}{r^2} + k^2, \quad Q_2 = S_B \frac{B^2 k^2}{r^2}, \quad Q_3 = \frac{2k^2}{r^2} (1 + B^2).$$

We multiply equation (10) by the complex conjugate of δu_r , δu_r^\dagger and integrate between r_0 and infinity. Boundary terms vanish, so

$$\gamma^2 \left[\left(\frac{d \delta u_r}{dr} \right)^2 + Q_1 |\delta u_r|^2 \right] + \gamma Q_2 |\delta u_r|^2 + Q_3 |\delta u_r|^2 = 0, \quad (11)$$

where $|\delta u_r|^2 = \int_1^\infty dr \delta u_r \delta u_r^\dagger \geq 0$ is non-negative, as is $(d \delta u_r / dr)^2$.

Equation (11) is a quadratic in γ whose roots depend crucially on S_B . When $S_B = 0$ (the inviscid limit), γ is purely imaginary (neutrally stable, travelling waves), whereas when $S_B > 0$ the result is quite different. In this

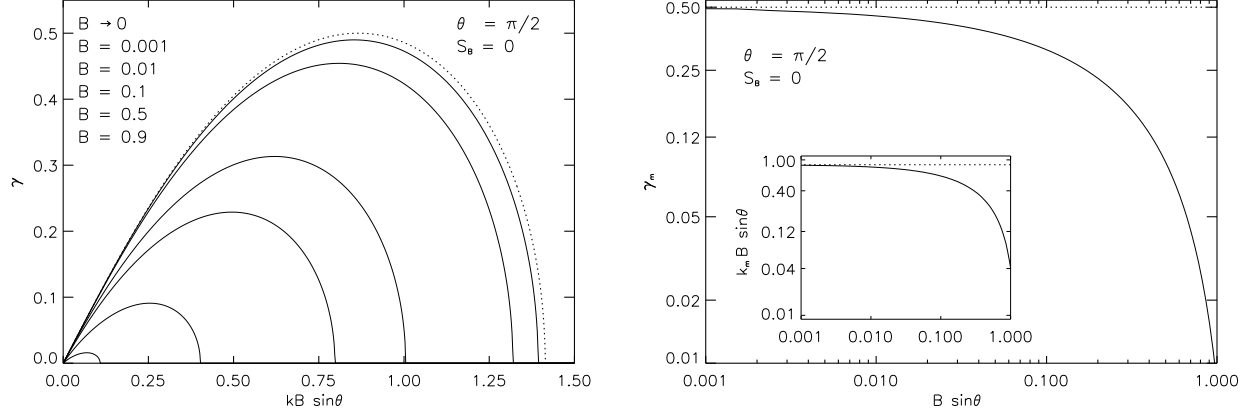


Figure 2. *Left panel:* Growth rate of the $n=0$ (fastest) branch of the inviscid global MRI as a function of the vertical Alfvén frequency $kB \sin \theta$ for several values of B (time and length are non-dimensionalised with respect to r_0 and Ω_0). In the weak field limit, we recover the behaviour of the local MRI (dotted line). For all figures, the top-to-bottom order of the varied parameter corresponds to the top-to-bottom order of the main-panel curves. *Right panel:* Maximum growth rate γ_m as a function of $B \sin \theta$. As $B \rightarrow 0$, γ_m asymptotes to the local Oort-A maximum $= 1/2$ (dotted line). Inset: The wavenumber k_m at which γ_m occurs as a function of B along with the local maximum $\sqrt{3}/4$ (dotted line). Note: In the inviscid weak-field limit, two configurations with the same vertical magnetic field will exhibit identical behaviour – Section 5.3

case $\mathcal{R}(\gamma) < 0 \forall S_B$ and the only question is whether perturbations are purely damped, or damped and travelling.

It follows that if the system is stable in the absence of the Braginskii viscosity, it remains so in its presence.

4 VERTICAL FIELD, $\theta = \pi/2$

4.1 Inviscid MRI, $S_B = 0$

For simplicity, we start by considering the inviscid limit of a purely vertical field $\mathbf{B} = B_z \hat{\mathbf{e}}_z$, i.e. $\theta = \pi/2, S_B = 0$. In this case equations (6) to (8) simplify⁵:

$$K_{ivn}(k) = 0, \quad (12)$$

with

$$v_n^2 \equiv - \left[\frac{2k^2}{\gamma^2 + \sigma^2} \frac{(\gamma^2 - \sigma^2)}{(\gamma^2 + \sigma^2)} + 1 \right]. \quad (13)$$

If $v_n^2 < 0$, $K_{ivn}(k)$ has no nontrivial zeros and it follows that for an instability $v_n^2 > 0$ (hence our sign convention in equation (6)). This implies γ^2 is bounded from above by σ^2 .

Numerical solutions to equations (12) and (13) are obtained using Newton's method (implemented in Mathematica). There is an unstable solution (and three stable ones) which is shown in Fig. 2. We find γ is real, positive, and of order the shear rate. The instability is the global MRI, and the $n = 0, v_0$ branch has the largest growth rate.

The fastest growing modes have $k \sim 1/B$, so in the strong field regime $B \lesssim 1, k \gtrsim 1$ the mode is large scale (physically, smaller scale modes are suppressed by magnetic tension) and is peaked away from the inner boundary. The

result is that γ_m is reduced below the Oort-A maximum that occurs when $B \sim 1/k \ll 1$ and the mode is localised at $r = 1$ (Curry et al. 1994).

In this weak field regime the problem is amenable to asymptotic analysis. It has been shown by Cochran (1965) and Ferreira & Sesma (1970, 2008) that in this limit, the zeros of $K_{ivn}(k)$ are given by

$$v_n \sim k + s_n 2^{-1} k^{\frac{1}{3}} + \dots, \quad (14)$$

where $s_n = a_n 2^{\frac{2}{3}}$, a_n is the modulus of the n^{th} real negative zero of the Airy function Ai (Abramowitz & Stegun 1964) and omitted terms are of the form k^b with $b < 1/3$. This result can be used to find the asymptotic-in- k form of γ by inverting equation (13) to form a bi-quadratic

$$\gamma^4 + 2 \left(\sigma^2 + \frac{k^2}{1 + v_n^2} \right) \gamma^2 + \sigma^2 \left(\sigma^2 - 2 \frac{k^2}{1 + v_n^2} \right) = 0, \quad (15)$$

into which we substitute equation (14). Retaining the first two terms in v_n , we solve exactly for γ^2

$$\gamma^2 = -\sigma^2 + \left(1 - s_n k^{-\frac{2}{3}} \right) \left(-1 \pm \sqrt{\frac{1 + 4\sigma^2}{1 - s_n k^{-\frac{2}{3}}}} \right), \quad (16)$$

in which the positive root corresponds to the instability. Numerically we find the fastest growing mode (for a given B, S_B), γ_m and the wavenumber at which it occurs k_m , obey $\partial \gamma_m / \partial B, \partial (k_m B) / \partial B < 0$.

To draw an analogy with the local approximation (see Section 6.3), n that indexes the number of zeros in the domain is like a radial wavenumber. For large enough n , the solutions are plane waves. To see this, we apply a WKB analysis to equation (6) using the small parameter $kr/v_n \equiv x/v_n \ll 1$ (Dubrulle & Knobloch 1993; Ogilvie 1998). We have

$$\frac{d^2 \delta u_r(x)}{dx^2} + \frac{v_n^2}{x^2} \delta u_r(x) = 0. \quad (17)$$

Demanding that δu_r is real, this has solutions

$$\delta u_r = \sqrt{x} \cos(v_n \ln x), \quad (18)$$

⁵ Equations (12) and (13) correspond to equations (3.4) and (3.5) of Curry et al. (1994) with $a = 1$ and equations (30) and (31) of Dubrulle & Knobloch (1993) who have already solved this problem.

and to ensure $\cos(v_n \ln x) = 0$ at $r = 1$, it must satisfy the boundary condition

$$v_n \ln k = \left(n + \frac{1}{2}\right) \pi, \quad (19)$$

which determines the spectrum of solutions.

Combining equations (13) and (19) we have

$$\gamma^2 = -\sigma^2 + \alpha \left(-1 + \sqrt{1 + 4\sigma^2 \alpha^{-1}}\right), \quad (20)$$

where $\alpha = k^2 (\ln k)^2 / n^2 \pi^2$ and we have neglected factors of $1/2 \ll n$.

In the large n limit, on small enough scales, the mode structure given by equation (18) is especially simple. Reverting to r as our radial coordinate, we expand equation (18) about $r = r_1 \sim \mathcal{O}(1)$. To leading order we find

$$\delta u_r = \mathcal{A} \left(1 + \frac{1}{2} \frac{r}{r_1}\right) \cos\left(\frac{v_n}{r_1} r + \xi\right), \quad (21)$$

where $\mathcal{A} = \sqrt{k r_1}$ and $\xi = v_n \ln k r_1$.

These solutions describes rapidly oscillating modes with frequency v_n and a slowly varying amplitude $\propto \mathcal{A}$. For sufficiently large v_n , the solutions are plane waves whose growth rate decreases with n .

4.2 Viscous MRI, $S_B \neq 0$

Allowing for viscosity whilst retaining a vertical field, equations (7) and (8) again reduce to a simple form:

$$p^2 \equiv k^2 \frac{\gamma^2 + \sigma^2}{\gamma^2 + \sigma^2 + S_B \gamma \sigma^2}, \quad (22)$$

$$v_n^2 \equiv - \left[\frac{2k^2}{\gamma^2 + \sigma^2 + S_B \gamma \sigma^2} \frac{(\gamma^2 - \sigma^2)}{(\gamma^2 + \sigma^2)} + 1 \right]. \quad (23)$$

Unlike the inviscid case, we can no longer *guarantee* the reality of p as γ can, and indeed sometimes does, take complex values. The problem is generally not of Sturm-Liouville form and so the roots of $K_{ivn}(p)$ are complex.

Numerically we again find four branches of which three are stable, and one unstable. The unstable mode (the only one of interest) is real, so if $\Re(\gamma) > 0$ then $\gamma \in \Re$. In this case, the problem is Sturm-Liouville. The unstable branch can be traced from the inviscid MRI (and is maximized for $n = 0, v_0$), Figs. 1, 3 and 5.

Asymptotic expressions for γ and k can be found using the results of Cochran (1965) and Ferreira & Sesma (2008) for the (complex) roots of equation (9):

$$v_n \sim \pi / (\ln 2 - \gamma_{\text{Euler}} - \ln p), \quad p \in \mathbb{C}, |p| \ll 1, \quad (24)$$

$$v_n \sim p + a_n 2^{-\frac{1}{3}} p^{\frac{1}{3}} + \dots, \quad p \in \mathbb{C}, |p| \gg 1, \quad (25)$$

where $\gamma_{\text{Euler}} \simeq 0.58$ is the Euler constant.

For $S_B \gg 1$ we combine equations (22) and (23) to get

$$\begin{aligned} \frac{\gamma^4}{k^4} + \frac{\gamma^2}{k^2} \left(\text{Re}^{-1} \gamma + \frac{2}{1 + v_n^2} + 2B^2 \right) \\ + B^2 \left(\text{Re}^{-1} \gamma - \frac{2}{1 + v_n^2} + B^2 \right) = 0 \end{aligned} \quad (26)$$

where $\text{Re}^{-1} = S_B B^2$ is the inverse of the Reynolds number.

We expand equation (26) in $\gamma^2/k^2 \sim \epsilon \ll 1$ and solve $\gamma = \gamma_0 + \epsilon \gamma_1 + \dots$ order by order. To lowest order we find

$$\gamma_0 = \text{Re} \left(\frac{2}{1 + v_n^2} - B^2 \right),$$

and to $\mathcal{O}(\epsilon)$

$$\gamma_1 = -\frac{1}{B^2} \left[\gamma_0 + 2 \text{Re} \left(\frac{1}{1 + v_n^2} + B^2 \right) \right],$$

and so

$$\gamma \simeq \text{Re} \left(\frac{2}{1 + v_n^2} - B^2 \right) - \frac{\gamma_0^2}{k^2 B^2} \left[\gamma_0 + 2 \text{Re} \left(\frac{1}{1 + v_n^2} + B^2 \right) \right]. \quad (27)$$

Numerically we find $k_m \ll 1$ which, combined with equations (22) and (24), implies $v_n \simeq -\pi / \ln k$. It follows that to lowest order

$$\gamma_m = \text{Re}(2 - B), \quad S_B \gg 1, \quad (28)$$

and, differentiating equation (27) with respect to k and neglecting leading order logarithmic variations,

$$k_m \simeq \frac{2 - B^2}{B\pi} \sqrt{2 + \frac{B^2}{2} \text{Re}(\ln \text{Re}^{-1})^{3/2}}, \quad S_B \gg 1. \quad (29)$$

For $S_B, B \ll 1$, equation (25) applies and so γ is governed by

$$(\gamma^2 + \sigma^2)^2 + [2 - k^{-2} (S_B \gamma \sigma^2 - 2)] (\gamma^2 - \sigma^2) = 0,$$

where we have used $v_n \simeq k \gg 1$. We expand in $1/k^2 \ll 1$ so $\gamma = \gamma_0 + k^{-2} \gamma_1 + \dots$, and again solve order by order. To lowest order we find γ_0 satisfies the inviscid equation

$$\gamma_0 = \sqrt{-(\sigma^2 + 1) + \sqrt{1 + 4\sigma^2}}, \quad S_B \ll 1, \quad (30)$$

and at $\mathcal{O}(k^{-2})$

$$\gamma_1 = \frac{-\gamma_0^2 (1 + S_B \gamma_0 \sigma^2) + \sigma^2 (1 - S_B \gamma_0 \sigma^2)}{4(\gamma_0 + \sigma)^3 + \gamma_0}, \quad S_B \ll 1. \quad (31)$$

To see the effect of variations in n on γ we perform a WKB analysis in which we order $v_n \gg k \gg 1 \gg S_B$ so $\ln p / v_n$ is a small parameter – see Section 4.1. The boundary condition for the viscous modes is then

$$v_n \ln \left[k \left(1 - \frac{1}{2} \frac{S_B \gamma \sigma^2}{\gamma^2 + \sigma^2} \right) \right] = \left(n + \frac{1}{2} \right) \pi.$$

Combining this with equation (23), we expand in $S_B \ll 1$ so $\gamma = \gamma_0 + S_B \gamma_1 + \dots$. To lowest order γ_0 is given by the inviscid equation (20), and to $\mathcal{O}(S_B)$

$$\gamma_1 = \frac{-\gamma_0 \sigma^2 \sqrt{\gamma^2 + \sigma^2}}{4(\gamma_0 + \sigma)^3 + 2\alpha \gamma_0} < 0, \quad v_n \gg 1, S_B \ll 1. \quad (32)$$

In the various limits, our asymptotics confirm the numerical results that $\gamma \in \Re$, and $\partial \gamma / \partial S_B < 0$. Contrasting the results of this section with the inviscid case when $B \ll 1$, we have

$$S_B \rightarrow 0, \quad \gamma_m \simeq 1/2, \quad k_m \simeq B^{-1} \sqrt{3/4},$$

$$S_B \rightarrow \infty, \quad \gamma_m \simeq S_B^{-1} B^{-2}, \quad k_m \simeq S_B^{-1} B^{-3} (\ln S_B B^2)^{3/2}.$$

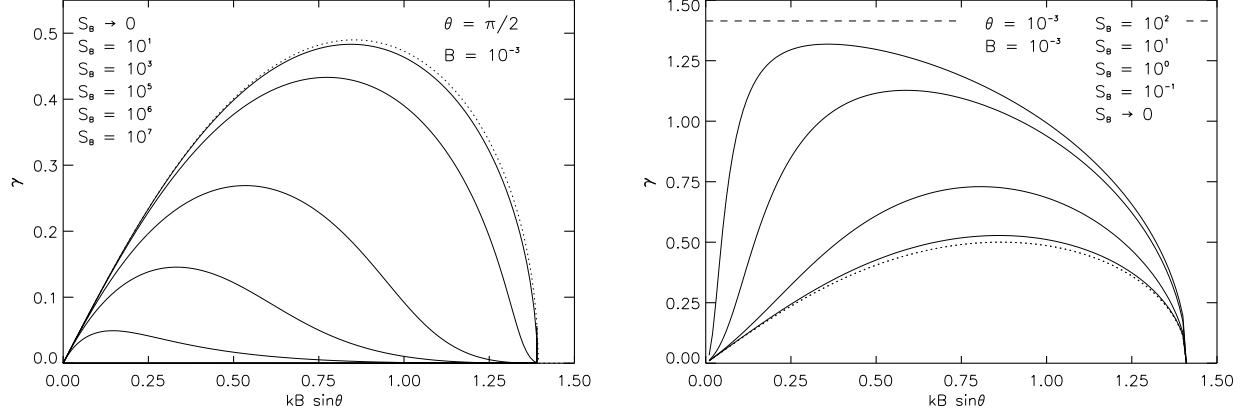


Figure 3. Growth rate of the $n=0$ (fastest) branch of the global MRI with Braginskii viscosity for a two different weak, $B = 10^{-3}$, field configurations and a range of S_B . *Left panel:* Vertical Field: For fixed k , γ decreases as S_B increases and is bounded above by the inviscid growth rate (dotted line), but the critical wavenumber above which $\gamma < 0$ is independent of S_B . *Right panel:* Slightly pitched field: In contrast to $\theta = \pi/2$, for a given k , the viscous case $\gamma(S_B \neq 0) > \gamma(S_B = 0)$ inviscid case (dotted), but is less than the local Lorentz-force free, or MVI, limit (dashed). As $S_B \rightarrow \infty$, $k_m \rightarrow 0$ but, unlike the vertical case, $\gamma_m \rightarrow \sqrt{2}$.

5 PITCHED FIELD, $\theta \ll 1$

5.1 Ordering assumptions

When the magnetic field has both a vertical and an azimuthal component, the perturbed Braginskii stress tensor exerts an azimuthal ‘tension’ force on separating plasma elements. For arbitrary θ , the system is neither Sturm-Liouville (equation (6) is complex) nor is it amenable to the kind of polynomial inversion used in Section 4.

However, assuming $\theta \ll 1$ matters simplify considerably. Physically, this choice of pitch angle represents the most realistic non-isolated galactic magnetic field configuration (Beck et al. 1996). Mathematically, as we now show, it is a singular limit that constitutes the stability threshold between actively damped modes, Section 3, and an unstable configurations that grows even faster than the inviscid global MRI (to which the following stability threshold also applies)

Damped : $\theta = 0$, Unstable : $\theta \sim \epsilon$.

Here $\epsilon \ll 1$ is a small parameter with respect to which we order the pitch angle and the remaining quantities in equation (6): $\gamma, k, d/dr, B$ and S_B .

Letting $\theta \sim \epsilon$ we can retain only the first few terms in a series expansion of our trigonometric functions

$$\cos \theta = 1 - \frac{\theta^2}{2} + \mathcal{O}(\theta^4), \quad \sin \theta = \theta - \frac{\theta^3}{6} + \mathcal{O}(\theta^5).$$

To include their effects, we assume a strong magnetic field $B \sim \mathcal{O}(1)$ and Braginskii viscosity $S_B \sim \mathcal{O}(1)$. To retain vertical magnetic tensions $\sigma = kB \sin \theta$ to order 1 (failing to do so removes the high wavenumber cutoff and leaves the equations ill-posed), we set $k \sim 1/\epsilon$. Then, in anticipation of unstable modes that grow at the shear rate, we order $\gamma \sim 1$ too. Balancing terms in equation (6), we find $d/dr \sim p \sim k \sim 1/\epsilon$.

In summary, our orderings are

$$\theta \sim \epsilon, \quad \gamma \sim \sigma \sim B \sim S_B \sim 1, \quad k \sim \frac{d}{dr} \sim \epsilon^{-1}. \quad (33)$$

We apply these scalings to equations (6) to (8) and retain the lowest order ϵ terms. We find δu_r is still governed by Bessel’s equation and, since $p \equiv k$, γ is determined by equation (12) and

$$v^2 \equiv -\frac{1}{E_1}(\gamma^4 + b_3\gamma^3 + b_2\gamma^2 + b_1\gamma + b_0), \quad (34)$$

where

$$\begin{aligned} E_1 &= (\sigma^2 + \gamma^2)(\sigma^2 + \gamma^2 + S_B\gamma\sigma^2), \\ b_3 &= S_B\sigma^2\theta^{-2}, \\ b_2 &= 2k^2(1 + B^2) - 4iS_B\sigma^2k\theta^{-1}, \\ b_1 &= -S_B\sigma^2k^2(2 + B^2) - 8i\sigma k^2B, \\ b_0 &= -2\sigma^2k^2(1 + B^2). \end{aligned}$$

We start by solving the inviscid problem.

5.2 Pitched inviscid MRI. $S_B = 0$

In the inviscid weak-field regime, we recover the vertical weak-field instability of Section 4.1 and Fig. 2. B appears via the vertical Alfvén frequency only so $k_m(\theta = \pi/2)/k_m(\theta = \text{tilted}) = 1/\theta \gg 1$ so the unstable mode will be confined to a boundary layer of width $\sim 1/(B\theta) \sim \mathcal{O}(\epsilon^2)$.

If B is small but finite (implicitly all orderings are subsidiary to equation (33)) the governing dispersion relation is the complex quartic⁶

$$(\gamma^2 + \sigma^2)^2 + 2(1 + B^2)(\gamma^2 - \sigma^2) - 8iB\sigma\gamma = 0.$$

Writing γ as a series in $B \ll 1$ we find

$$\gamma \simeq 2i \frac{B\sigma}{\sqrt{4\sigma^2 + 1}} + \sqrt{\left(\sqrt{4\sigma^2 + 1} - \sigma^2 - 1\right)}, \quad (35)$$

⁶ Solutions to this polynomial are considered in detail in Curry & Pudritz (1995) and further discussion can be found in Knobloch (1992).

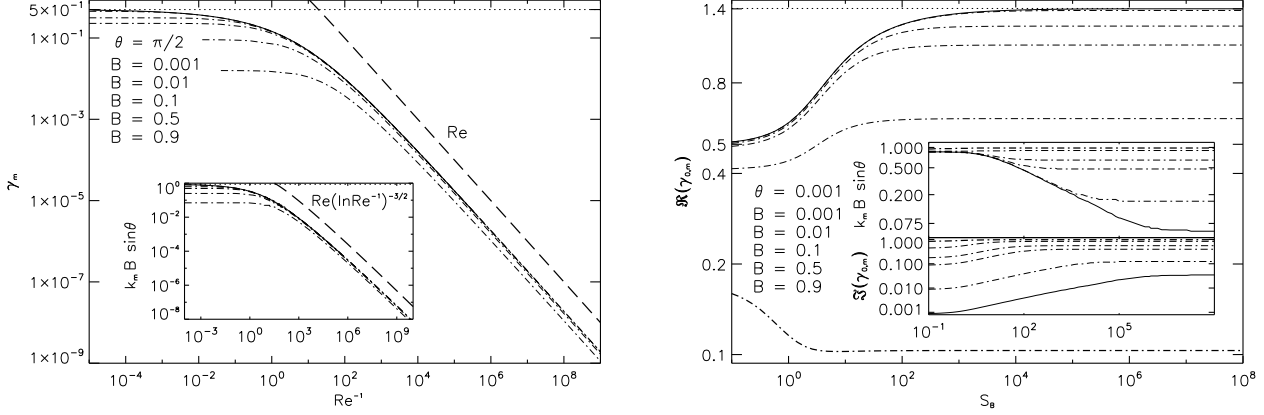


Figure 4. $\Re(\gamma_m)$, $\Im(\gamma_m)$ (if it exists), and the corresponding vertical Alfvén frequency $k_m B \sin \theta$ for two field configurations. *Left panel:* Vertical field: $\gamma_m \in \mathbb{R}$ and $k_m B \sin \theta$ vs. $\text{Re}^{-1} = S_B B^2$ for a range of B . These are bounded above by the $B \ll 1$ local limits of $1/2$ and $\sqrt{3/4}$ (dotted lines), and well matched by the asymptotic results (dashed lines) given by equations (28) and (29). *Right Panel:* Slightly pitched, $\theta = 10^{-3}$: $\Re(\gamma_m)$ and $k_m B \sin \theta$ are bounded from above by the local $B \ll 1$ limit of $\sqrt{2}$ (main panel, top dotted line) and the inviscid limit $\sqrt{3/4}$ (top inset, dotted line). The imaginary part of the growth rate $\Im(\gamma_m)$ (bottom inset) is well described in the small and large S_B limits by equations (36) and (48). Note that $\partial \gamma_m(B \sim 1)/\partial S_B < 0$ (bottom curve, main panel) demonstrates the combined effects of hoop tension and the Braginskii viscosity.

with a maximum value

$$\gamma_m = \frac{1}{2} + i\sqrt{\frac{3}{4}}B, \quad (36)$$

which occurs at $k_m = \sqrt{3/4}B^{-1}$, Fig. 4.

5.3 Pitched MRI with Braginskii viscosity, $S_B \neq 0$

In the presence of the Braginskii viscosity we find a complex instability whose real part exceeds that of its inviscid counterpart. Numerical solutions described by equations (12) and (34) are shown in Figs. 3, 4 and 5. When $B \rightarrow 0, S_B \rightarrow \infty$ the growth rate tends to the shear rate $\Re(\gamma) \rightarrow \sqrt{2}d \ln \Omega / d \ln r = \sqrt{2}$ and, as before, the fastest growing modes occur for $n = 0$.

Asymptotic expressions for γ and k can be found by substituting equation (14) into equation (34). For $B \ll 1$, γ is governed by

$$(\gamma^2 + \sigma^2)^2 + 2(\gamma^2 - \sigma^2) + S_B \sigma^2 \gamma (\gamma^2 + \sigma^2 - 2) = 0.$$

Differentiating this with respect to σ (k, B and θ appear together only in one combination and so σ is treated as a single independent variable), and setting $d\gamma/d\sigma = 0$, the stationary points of γ obey:

$$S_B \gamma^3 + 2\gamma^2 + 2S_B(\sigma^2 - 1)\gamma + 2(\sigma^2 - 1) = 0. \quad (37)$$

By considering the branch σ_m that maximizes the stationary value of γ , and introducing $\zeta_m = \sigma_m^2$, we find

$$\zeta_m = \frac{S_B \gamma_m (2 - \gamma_m^2) + 2(1 - \gamma_m)}{2(\gamma_m S_B + 1)}, \quad (38)$$

and substituting this into equation (37) we obtain a polynomial whose solutions describe γ_m :

$$\gamma_m^6 - 4\gamma_m^4 + 4(1 - 4S_B^{-2})\gamma_m^2 + 4S_B^{-1}(2\gamma_m + S_B^{-1} - 5\gamma_m^3) = 0. \quad (39)$$

Because it is a sixth order polynomial, there is no general formulae for its roots. However, the presence of the

asymptotic parameter S_B recommends a series solution. The power of the expansion parameter S_B depends on whether it is large or small.

Taking $S_B \ll 1$ first, we write

$$\gamma_m = \gamma_{m,0} + S_B \gamma_{m,1} + \mathcal{O}(S_B^2), \quad (40)$$

$$\zeta_m = \zeta_{m,0} + S_B \zeta_{m,1} + \mathcal{O}(S_B^2). \quad (41)$$

Substituting equation (40) into equation (39), and solving order by order, we find, to lowest order $\gamma_{m,0} = 1/2$. To next order $\gamma_{m,1} = 3/32$ and so

$$\gamma_m = \frac{1}{2} \left(1 + S_B \frac{3}{16} \right), \quad S_B \ll 1. \quad (42)$$

Substituting this into equations (38) and (41), we find $\sigma_m = \sqrt{3/4}(1 - S_B/48)$, so the most unstable mode is

$$k_m = \frac{1}{B\theta} \sqrt{\frac{3}{4}} \left(1 - S_B \frac{1}{48} \right) \quad S_B \ll 1. \quad (43)$$

Now taking $S_B \gg 1$, we write

$$\gamma_m = \gamma_{m,0} + S_B^{-1/2} \gamma_{m,1} + S_B^{-1} \gamma_{m,2} + \mathcal{O}(S_B^{-3/2}), \quad (44)$$

$$\zeta_m = \zeta_{m,0} + S_B^{-1/2} \zeta_{m,1} + S_B^{-1} \zeta_{m,2} + \mathcal{O}(S_B^{-3/2}). \quad (45)$$

Following the same procedure, to lowest order $\gamma_{m,0} = \pm\sqrt{2}, 0$ and we take the positive root corresponding to the instability. At first order we obtain no information, but at second order we find that $\gamma_{m,1} = \pm 2^{3/4}/3^{1/2}$. Taking the negative root (see Fig. 5) we have

$$\gamma_m = \sqrt{2} \left(1 - \left(\frac{2}{9} \right)^{1/4} S_B^{-1/2} \right), \quad S_B \gg 1. \quad (46)$$

Substituting this and equation (45) into equation (38), to lowest order $\zeta_{m,0} = 0$, and at next order $\zeta_{m,1} = 2^{5/2}/3^{1/2}$ so $\sigma_m = (2^5/9)^{1/8} S_B^{-1/4}$, and

$$k_m = \frac{1}{B\theta} \left(\frac{2^5}{9} \right)^{1/8} S_B^{-1/4}, \quad S_B \gg 1. \quad (47)$$

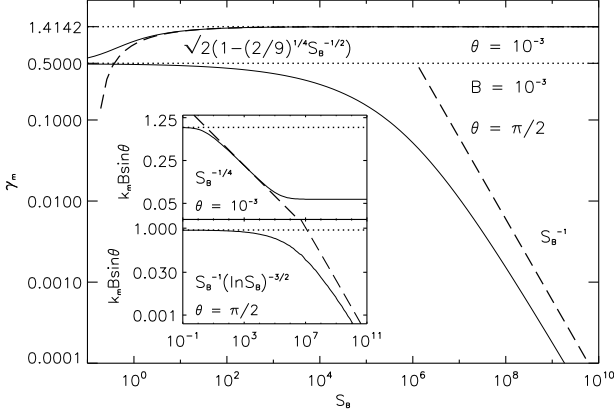


Figure 5. Direct comparison of the γ_m (main panel) and $k_m B \sin \theta$ (insets) behaviour of the unstable mode for $\theta = 10^{-3}$ (top solid line and inset) and $\theta = \pi/2$ (bottom solid line and inset) with S_B for a weak magnetic field, $B = 10^{-3}$. The dotted lines are the local maxima, and the dashed lines are the asymptotic scalings given by equations (28) and (46) for γ_m , and equations (29) and (47) for $k_m B \sin \theta$.

Now considering the effect of finite magnetic fields, $\Re(\gamma_m)$ (and $\Im(\gamma_m)$ which is now present) increase with S_B . Guided by the numerical results, we assume $|\gamma| \sim 1$ and take the leading order balance of terms $\propto S_B \rightarrow \infty$ in equation (34). We find

$$\gamma^2 (\sigma^2 + B^2) - 4i\sigma B\gamma + \sigma^2 (\sigma^2 - B^2 - 2) = 0,$$

and the resultant growth rate is

$$\gamma = \frac{2iB\sigma + \sigma \sqrt{(B^2 - \sigma^2) - 2(B - \sigma)}}{B^2 + \sigma^2}, B \lesssim 1, S_B \gg 1, \quad (48)$$

which agrees well with the numerics, Fig. 4.

To see the effects of n on γ we adopt the same WKB approach and orderings as Section 4.2 where v_n is now given by the appropriate limit of equation (34). We assume $B \ll 1$ and expand in $S_B \ll 1$ so $\gamma = \gamma_0 + S_B \gamma_1 + \dots$. To lowest order γ_0 is given by equation (20), and to $\mathcal{O}(S_B)$

$$\gamma_1 = \frac{\gamma_0 \sigma^2 (2\alpha - \gamma_0^2 - \sigma^2)}{4(\gamma_0 + \sigma)^3 + 2\alpha\gamma_0} > 0, \quad (49)$$

so the Braginskii viscosity increases the growth rate beyond the inviscid limit.

Contrasting the results of this section with the inviscid case, for $B \ll 1$ we have

$$\begin{aligned} S_B \rightarrow 0, \quad \Re(\gamma_m) &\simeq 1/2, & k_m &\simeq (\theta B)^{-1} \sqrt{3/4}, \\ S_B \rightarrow \infty, \quad \Re(\gamma_m) &\simeq \sqrt{2} - S_B^{-1/2}, & k_m &\simeq (B\theta S_B^{1/4})^{-1}, \end{aligned}$$

with the caveat that $k_m \rightarrow 0$ only in the formal limit $B \rightarrow 0$ too (see Fig. 4 for the effect of finite B at large S_B).

Considering the effects of hoop tension, we find $\Im(\gamma)$ is an order of magnitude greater in the viscous limit. For example, we find numerically that $\Im(\gamma(S_B = 10^8))/\gamma(S_B = 0) \simeq 40$ for $B = 10^{-3}$ (which agrees with equations (36) and (48) to within half a percent for this and all other examples with $B \lesssim 0.5$, $S_B \gg 1$).

6 DISCUSSION

6.1 Physical mechanism

We have seen that the orientation of the magnetic field categorically determines the behaviour of the system. How is this to be understood physically?

The most informative explanation comes in the weak field regime where the role of the magnetic field is twofold. Firstly it facilitates the generation of pressure anisotropies proportional to its rate of change, or equivalently (in the collisional regime) $\propto \delta \mathbf{b} \mathbf{b} : \nabla \mathbf{u}$. Because collisions are involved this is a necessarily dissipative process. Equations (1) to (4) yield an energy conservation law

$$\begin{aligned} \frac{d}{dt} \left(\frac{\langle u^2 \rangle}{2} + \frac{\langle B^2 \rangle}{2} \right) &= -3\nu_B \langle |\mathbf{b} \mathbf{b} : \nabla \mathbf{u}|^2 \rangle, \\ &= -3\nu_B \left\langle \left(\frac{d \ln B}{dt} \right)^2 \right\rangle, \end{aligned}$$

where $\langle \cdot \rangle$ are volume averages.

That is, the Braginskii viscosity damps any motions that change the magnetic field strength. This is the first role of the magnetic field.

The second role of the magnetic field is a geometric one. Assuming anisotropies do arise (from changes in the magnetic field strength), the field's orientation dictates the projection of the anisotropic stress onto the fluid elements of the plasma, thereby affecting their dynamics. As we now explain, this fact is crucial in determining the stability, or lack thereof, and the role global effects have on a differentially rotating magnetized plasma.

When the field lines have both vertical and azimuthal components (it is pitched) fluid elements at different heights can exert an azimuthal stress on each other. The sign of this stress can be either positive or negative. If the magnetic field is unstable, so its rate of change is positive, the anisotropic stress acts to oppose any azimuthal separation of the two elements (this can be identified as the fluid version of the stress responsible for the microscopic mirror force). In this case, like the MRI, velocity perturbations to fluid elements at different heights increase (decrease) their angular momentum causing them to move to larger (smaller) radii. In a system with an outwardly decreasing angular velocity profile, this leads to an azimuthal separation of the fluid elements. The associated magnetic field growth ensures the stress is of the right sign to oppose this separation and this transfers angular momentum between them in a way that facilitates further (radial) separation; i.e. an instability (see Quataert et al. (2002) for a physical explanation including a spring analogy). This is the second role of the magnetic field.

In conjunction, the two roles explain our results. In isolated field geometries where there is no projection of the stress onto fluid elements at different heights, the Braginskii viscosity does not give rise to an instability; its only effect is dissipative (Kulsrud 2005; Lyutikov 2007; Kunz et al. 2011). This accounts for the damping of perturbations in the azimuthal configuration. It also accounts for the reduced growth rate of the vertical MRI (that depends on the Maxwell, not the Braginskii, stress), along with the increased radial extent of the mode away from the region of maximum shear (Curry et al. 1994). When the field is

pitched its dissipative effects persist, but the free energy contribution from the differential shear flow will *always* be greater, leading to an instability (the dissipative effects cannot change the stability boundary, just the growth rate). Of course the total, equilibrium plus perturbed, field energy will decrease if viscosity is present (and viscous heating is not) but, from the perspective of generating turbulence or transporting angular momentum, this is a secondary consequence.

Now considering finite magnetic field strengths (and therefore hoop tension and viscous curvature stresses) we find these modes become over-stable. The variation of the travelling wave component of the unstable mode is simply a combination of these two effects, to varying degrees.

6.2 Astrophysical example

The mathematical results in this paper should be applicable to any collisional magnetized disc with a decreasing angular velocity profile. However, it is helpful to provide a physical example where our analysis holds. Because our theory is developed for a disc with an angular velocity profile $\propto r^{-1}$ we choose the ISM of a spiral galaxy where a range of analytic and numerical studies already exist (Kim et al. 2003; Kitchatinov & Rüdiger 2004; Dziourkevitch et al. 2004; Piontek & Ostriker 2005; Wang & Abel 2009).

Further motivation to study this system comes from Sellwood & Balbus (1999) who have argued that in the HI region outside the optical disc of a spiral galaxy, the velocity dispersion measurements of $\sim 5 - 7 \text{ km s}^{-1}$ may be driven by the differential rotation of the disc, mediated by the MRI.

On this basis, we consider the warm ISM in the quiescent regions of a typical spiral galaxy where the plasma is generally subject to a weak magnetic field and an outwardly decreasing angular velocity profile. It is also magnetized, and so subject to the effects of the Braginskii viscosity. This last feature can be seen, and the other relevant parameters estimated, by adopting the following set of fiducial parameters for the ISM (Binney & Tremaine 1988; Beck et al. 1996; Ferrière 2001). These are in agreement with NGC1058, the well studied face-on disc galaxy considered by Sellwood & Balbus (1999).

Reverting to dimensionalised units for clarity, we have:

- Particle number density (ion and electron are the same)
 $n \sim 0.3 \text{ cm}^{-3}$.

- Temperature (we assume ions and electrons are in thermal equilibrium)

$$T_i \sim 5 \times 10^4 \text{ K};$$

consequently the ion thermal speed is

$$v_{\text{th}i} = \left(\frac{2T_i}{m_i} \right)^{1/2} \sim 3 \times 10^6 \text{ cm s}^{-1};$$

(T_i is in erg.)

- The ion-ion collision frequency (in seconds, assuming n in cm^{-3} , T_i in K and the Coulomb logarithm $\ln \Lambda = 25$) is⁷

$$\nu_{ii} \sim 1.5nT_i^{-3/2} \sim 4 \times 10^{-8} \text{ s}^{-1};$$

⁷ The full expression for the ion-ion collision frequency (ion-

consequently the mean free path is

$$\lambda_{\text{mfp}} = \frac{v_{\text{th}i}}{\nu_{ii}} \sim 7 \times 10^{13} \text{ cm}.$$

- The typical rotation rate of a spiral galaxy is

$$\Omega \sim 5 \times 10^{-16} \text{ s}^{-1}.$$

A typical value for the outer edge of the optical disc where the turbulence cannot be generated by stellar processes is

$$r \sim 3 \times 10^{22} \text{ cm},$$

and even within the optical disc, at the corotation radius in between the spiral arms, magnetized shear instabilities may be important (A. Shukurov – private communication).

Outside the optical disc a reasonable value for the vertical scale-height is

$$H \sim 10^{21} \text{ cm},$$

and so the disc is thin. The measured system-scale rotation (not turbulent) velocity is

$$U \sim 2 \times 10^7 \text{ cm s}^{-1}.$$

- The observed mean magnetic field strengths vary between galaxies but on the lower end of the scale are, at the present time (Beck et al. 1996)

$$B \sim 8 \times 10^5 \text{ cm s}^{-1} \quad - \text{ present.}$$

However, if the MRI is the dominant turbulence generating mechanism in the ISM, this value must represent the saturated state of the magnetic field. Assuming, as one must, that present field strengths have been amplified over time, at some earlier time they were weaker, e.g. Malyshkin & Kulsrud (2002); Kitchatinov & Rüdiger (2004).

To ensure the most unstable modes exist at scales $> \lambda_{\text{mfp}}$ so our theory is fluid-like we adopt the following value for the historical ‘initial’ field strength and lay aside the problem of where this came from (Kulsrud 1999; Brandenburg & Subramanian 2005),

$$B \sim 80 \text{ cm s}^{-1} \quad - \text{ initial.}$$

If we considering a plasma in this era, or the ISM in a galaxy where the magnetic field is not saturated, the plasma beta is

$$\beta = \frac{v_{\text{th}i}^2}{B^2} \sim 1.3 \times 10^9;$$

the ion cyclotron frequency is

$$\omega_i = \sqrt{\frac{4\pi n}{m_i}} \frac{eB}{c} \sim 2 \times 10^{-6} \text{ s}^{-1};$$

(e is the elementary charge, c the speed of light) and the ion Larmor radius is

$$\rho_i = \frac{v_{\text{th}i}}{\omega_i} \sim 1.5 \times 10^{12} \text{ cm};$$

and so the plasma is magnetized $\omega_i \gg \nu_{ii}$ (and will become even more so if the magnetic field becomes stronger).

electron collisions are sub-dominant for a thermalised plasma) is given by $\nu_{ei} = 4\sqrt{\pi}ne^4 \ln \Lambda / 3m_i^{1/2} T^{3/2}$ where e is the elementary charge and T is in erg (Braginskii 1965).

• The magnetic Prandtl number P_m is huge (and so we can take the Braginskii viscosity to be the only significant dissipative process)⁸:

$$P_m = \frac{\nu_B}{\eta} \simeq 7.5 \times 10^{-6} \frac{T^4}{n} \sim 7.5 \times 10^{13},$$

where η is the coefficient of resistivity and T is in K.

• The dimensionless parameter $S_B = 3\nu_B\Omega/(nm_iB^2) \simeq \beta\Omega/\nu_{ii}$ is

$$S_B \sim 1.1 \times 10^9 \frac{\Omega T^{5/2}}{B^2} \sim 42,$$

for the conditions above, so the Braginskii viscosity plays a role.

Our model of a gravitationally constrained, differentially rotating disc made up of an isothermal, incompressible, magnetized plasma fluid is consistent. Neglecting structure in z requires us to restrict our analysis to the galactic plane by considering vertical scales much less than the scale height of the disc $H \sim c_s/\Omega \sim$ where $c_s \sim v_{\text{thi}}$ is the isothermal sound speed.

Formally, both this and our remaining model assumptions can be expressed as a hierarchy of time-scales which are well satisfied for our set of parameters (we restrict attention to γ_m),

$$\frac{1}{\omega_i} \ll \frac{1}{\nu_{ii}} \ll \frac{1}{kc_s} \ll \frac{1}{\Omega} \ll \frac{1}{\Omega} \frac{r_0}{H}.$$

In order of increasing periods of time, these scalings correspond to: the plasma being magnetized; the plasma being collisional, i.e. a fluid; the model being uniform in the vertical direction; and the disc being thin, i.e. rotationally rather than pressure dominated.

The parameters in this section describe a physically realistic regime in which our analysis is valid, and potentially important in explaining the gas motions in parts of the ISM.

6.3 Relation to the local approximation

Because of its widespread use, we briefly comment on the relation of our results to the local analysis. In this approximation the coordinate system is Cartesian, the shear is modelled linearly, and the perturbed quantities are assumed to vary rapidly in the radial direction (with respect to the background variations) so they may be written as $\delta\mathbf{u}(r) = \delta\mathbf{u} \exp[i(lr + kz) + \gamma t]$, $lr \gg 1$. Under this assumption, a WKB analysis ignores terms proportional to $1/r$ and replaces d/dr by il . The local dispersion relation is (Islam & Balbus 2005; Ferraro 2007):

$$\gamma^4 + d_1\gamma^3 + d_2\gamma^2 + d_3\gamma + d_4 = 0, \quad (50)$$

where

$$\begin{aligned} d_1 &= S_B \sigma^2 \frac{l^2 + k^2 \cos^2 \theta}{l^2 + k^2}, \\ d_2 &= 2 \left(\sigma^2 + \frac{k^2}{l^2 + k^2} \right), \\ d_3 &= S_B \sigma^2 \left(\sigma^2 \frac{l^2 + k^2 \cos^2 \theta}{l^2 + k^2} - 2 \cos^2 \theta \frac{k^2}{l^2 + k^2} \right), \\ d_4 &= \sigma^2 \left(\sigma^2 - 2 \frac{k^2}{l^2 + k^2} \right). \end{aligned}$$

In the $k \gg l, l \gg k$ limits for $\theta = 0, \pi/2$ the local and global results are identical (modulo different boundary condition-dependent restrictions on the spectrum of allowed modes in the latter case).

However for $\theta \ll 1, B \lesssim 1$ the analyses differ. Locally we find unstable modes have $\gamma \in \mathbb{R}$, whilst globally γ is complex. Whilst in the inviscid limit $\Im(\gamma) \sim B$ can often be neglected. In the highly viscous limit $\Im(\gamma) \sim \sigma B/(\sigma^2 + B^2)$ and, as shown in Fig. 4, this can be over an order of magnitude greater. This difference may prove important (from a modelling perspective) for viscous systems which could have been treated locally, were they inviscid.

Furthermore, inconsistent with the global picture, for $\theta = 0, \pi/2$ and $l = 0$ the local analysis neglects the Braginskii viscosity. This can be understood from

$$\begin{aligned} \delta(\mathbf{bb} : \nabla \mathbf{u})_G &= \hat{\mathbf{e}}_\phi \cdot (\hat{\mathbf{e}}_\phi \cdot \nabla (\delta u_r \hat{\mathbf{e}}_r)) = \frac{\delta u_r}{r}, \quad \theta = 0, \\ \delta(\mathbf{bb} : \nabla \mathbf{u})_G &= \hat{\mathbf{e}}_z \cdot (\hat{\mathbf{e}}_z \cdot \nabla (\delta u_z \hat{\mathbf{e}}_z)) = ik \delta u_z, \quad \theta = \pi/2, \end{aligned}$$

whereas locally, assuming $\nabla \cdot \delta \mathbf{u} = i(k \delta u_z + l \delta u_r) = 0$ we have

$$\delta(\mathbf{bb} : \nabla \mathbf{u})_L = 0, \quad \theta = 0, \pi/2.$$

(Here the subscripts G and L stand for global and local.) Physically, in the global case, a component of the flow is projected along the magnetic field direction by the curvilinear geometry (azimuthal case) and the demands of the global incompressibility condition (vertical case), and so $|B|$ changes at linear order, thereby activating the Braginskii viscosity. This is not so in the local case.

One final clarification is worth noting. The local description predicts that the fastest growing unstable modes ($\theta \neq 0$) occur as $l \rightarrow 0$. Formally this is inconsistent with the assumption $l \gg 1/r \neq 0$ that went into deriving equation (50). The local solutions obtained under the WKB approximation are not self-consistent and should be described by the type of global solution we have constructed here. However, having determined the global solutions, we can confirm the $n = 0$ branch corresponds to γ_m , and so the local analysis is, at least qualitatively, correct in this respect.

7 CONCLUSION

The nature of the ideal MRI has been well established but how non-ideal modifications affect it remains an active topic of research (Blaes & Balbus 1994; Balbus & Terquem 2001; Kunz & Balbus 2004; Ferraro 2007; Pessah & Chan 2008; Devlen & Pekünlü 2010). Of interest to us, and the subject of this study, has been the global nature of the Braginskii-MHD MRI.

⁸ The coefficient of the Braginskii viscosity is given by $\nu_B = 0.96 n m_i v_{\text{thi}}^2 / \nu_{ii}$ and $\eta = 3 \sqrt{2 m_e / \pi c^2} \ln \Lambda e^2 T^{-3/2}$ where m_e is the electron mass and T is in erg (Spitzer 1962; Braginskii 1965).

Considering an isothermal, magnetized, collisional disc, perhaps the early ISM, we have found that for an azimuthal magnetic field with an asymptotically small vertical component, a singular instability emerges - the magnetized MRI. The growth rate of this instability $\sim \Omega$ depends on S_B , a dimensionless combination of the temperature, shear rate and Alfvén speed, and it is up to a factor of $2\sqrt{2}$ faster than its unmagnetized counterpart. In the limit where S_B is large, we determined the asymptotic maximum growth rate $\gamma_m \simeq \sqrt{2} \left(1 - S_B^{-1/2}\right)$ and corresponding wavenumber $k_m \simeq (\theta B)^{-1} S_B^{-1/4}$. As the field increases in strength the Larmor radius decreases $d\rho_i/dt \propto -\Omega$ (so the plasma becomes more magnetized) and as the azimuthal component of B increases, purely growing modes mutate into over-stabilities whose imaginary part also depends on S_B . Both of these factors may be important for the questions posed in Section 1, and for the turbulence that will eventually arise. In the early stages of the instability, before fully developed turbulence has set in, the instability will generate non-linear pressure anisotropies. What exact effect these will have is an open question, and so we finish with some thoughts on the subject.

One major uncertainty in the evolution of magnetized accretion discs is the effect of pressure anisotropy driven micro-instabilities whose growth rates are generally well in excess of the MRI e.g. mirror⁹ and firehose (Schekochihin et al. 2005). Although various models for treating them exist, a complete first-principles theory remains outstanding (Schekochihin & Cowley 2006; Sharma et al. 2006, 2007; Rosin et al. 2011). It is crucial for accretion theories to determine the fate of these instabilities fluctuations over long (transport) time-scales. This is because they determine the Maxwell and Braginskii stresses that, in turn, dictate the angular momentum transport (Shakura & Sunyaev 1973). Even if the pressure anisotropy is pinned at the marginal value for the microscale instabilities in some self-regularizing way, there are further complications that must be addressed.

Specifically, the viscous stress generated by the Braginskii viscosity can heat the plasma – at a rate $\propto (p_\perp - p_\parallel)^2$ (Kunz et al. 2011). Spatial inhomogeneities in the growth rate of the magnetic field, as one would expect in a turbulent system, will lead to inhomogeneities in the local pressure anisotropy, both in magnitude and sign. In regions of decreasing field strength the firehose would pin the anisotropy at $|(p_\perp - p_\parallel)/p| = 2/\beta$ and in regions of increasing field strength the mirror would pin it at $|(p_\perp - p_\parallel)/p| = 1/\beta$. The implication of this is that heating in regions of increasing and decreasing magnetic field strength could differ by a factor of \sim four and would occur on the decorrelation scale of the turbulent cascade’s viscous cut-off – where the shear is maximized (Schekochihin & Cowley 2006). If differential heating of this nature does occur then one might expect

⁹ In regions where $d \ln B / dt > 0$ slow-wave polarised modes (like the MRI) are unstable to the mirror with $\gamma_m \sim \omega_i (p_\perp - p_\parallel)/p$. For the set of parameters listed in Section 6.2 this is $\simeq 2 \cdot 10^{-22} \text{s}^{-1}$, a factor 10^6 slower than the MRI. However in many other contexts, e.g. the intracluster medium, the mirror can be up to a factor $\sim 10^8$ faster than the macroscopic shear rate (Hellinger 2007).

the non-linear dynamics to be further complicated by magnetized (and unmagnetized) temperature gradient instabilities, and the temperature dependence of both ν_B and the micro-instability thresholds (Balbus 2001; Quataert 2008; Schekochihin et al. 2010).

Understanding the rich interplay between these realisations of magnetized plasma phenomena constitutes an important and, as of yet, unsolved issue in astrophysics; specifically in accretion discs, but also in galaxies and galaxy clusters. The overall picture is a deeply interconnected one and the types of processes outlined above are probably pertinent, to some degree, to most magnetized astrophysical settings.

To address these issues there is a need for both non-linear simulations that include a wide range of magnetized physics, and a more complete theory of the transport effects of micro-instabilities. For the first task at least, this work should be useful for benchmarking global codes (Skinner & Ostriker 2010).

ACKNOWLEDGMENTS

We thank J. Binney, T. Heinemann, M. Kunz, G. Lesur, A. Nahum, G. Ogilvie, A. Schekochihin, A. Shukurov, J. Stone and O. Umurhan for useful discussions and suggestions at various stages of this project. This work was supported by a STFC studentship (MSR), DOE grant DE-FG02-05ER-25710 (MSR), and Leverhulme Trust International Network for Magnetized Plasmas (MSR).

REFERENCES

- Abramowitz M., Stegun I. A., 1964, Handbook of Mathematical Functions. Dover, New York
- Balbus S. A., 2000, ApJ, 534, 420
- Balbus S. A., 2001, ApJ, 562, 909
- Balbus S. A., 2003, ARA&A, 41, 555
- Balbus S. A., 2004, ApJ, 616, 857
- Balbus S. A., Hawley J. F., 1991, ApJ, 376, 214
- Balbus S. A., Hawley J. F., 1992, ApJ, 392, 662
- Balbus S. A., Hawley J. F., 1998, Reviews of Modern Physics, 70, 1
- Balbus S. A., Terquem C., 2001, ApJ, 552, 235
- Beck R., Brandenburg A., Moss D., Shukurov A., Sokoloff D., 1996, ARA&A, 34, 155
- Binney J., Tremaine S., 1988, Galactic dynamics. Princeton Univ Press, Princeton, NJ
- Blaes O. M., Balbus S. A., 1994, ApJ, 421, 163
- Braginskii S. I., 1965, Reviews of Plasma Physics, 1, 205
- Brandenburg A., Subramanian K., 2005, Phys. Rep., 417, 1
- Chandrasekhar S., 1960, Proceedings of the National Academy of Science, 46, 253
- Chandrasekhar S., 1961, Hydrodynamic and hydromagnetic stability. Clarendon Press, Oxford
- Chapman S., Cowling T. G., 1970, The mathematical theory of non-uniform gases
- Cochran J. A., 1965, Numerische Mathematik, 7, 238
- Curry C., Pudritz R. E., 1995, ApJ, 453, 697
- Curry C., Pudritz R. E., Sutherland P. G., 1994, ApJ, 434, 206

- Devlen E., Pekünlü E. R., 2010, MNRAS, 404, 830
- Dubrulle B., Knobloch E., 1993, A&A, 274, 667
- Dziourkevitch N., Elstner D., Rüdiger G., 2004, A&A, 423, L29
- Ferraro N. M., 2007, ApJ, 662, 512
- Ferreira E. M., Sesma J., 1970, Numer. Math, 16, 278
- Ferreira E. M., Sesma J., 2008, Journal of Computational and Applied Mathematics, 211, 223
- Ferrière K. M., 2001, Reviews of Modern Physics, 73, 1031
- Furukawa M., Yoshida Z., Hirota M., Krishan V., 2007, ApJ, 659, 1496
- Gammie C. F., Balbus S. A., 1994, MNRAS, 270, 138
- Goldreich P., Lynden-Bell D., 1965, MNRAS, 130, 97
- Goodman J., Xu G., 1994, ApJ, 432, 213
- Guan X., Gammie C., Simon J., Johnson B., 2009, The Astrophysical Journal, 694, 1010
- Hellinger P., 2007, Physics of plasmas, 14, 82105
- Islam T., Balbus S., 2005, ApJ, 633, 328
- Kersalé E., Hughes D. W., Ogilvie G. I., Tobias S. M., Weiss N. O., 2004, ApJ, 602, 892
- Kim W., Ostriker E. C., Stone J. M., 2003, ApJ, 599, 1157
- Kitchatinov L. L., Rüdiger G., 2004, A&A, 424, 565
- Knobloch E., 1992, MNRAS, 255, 25P
- Kulsrud R. M., 1999, ARA&A, 37, 37
- Kulsrud R. M., 2005, Plasma physics for astrophysics. Princeton University Press, N.J.
- Kunz M., Schekochihin A., Cowley S., Binney J., Sanders J., 2011, MNRAS, 410, 2446
- Kunz M. W., Balbus S. A., 2004, MNRAS, 348, 355
- Lifshitz E., Landau L., Pitaevskii L., 1984, Electrodynamics of continuous media. Pergamon Press
- Lyutikov M., 2007, ApJ Letters, 668, L1
- Malayshkin L. M., Kulsrud R. M., 2002, in Bulletin of the American Astronomical Society Vol. 34, Magnetized Turbulent Dynamo in Protogalaxies. p. 1194
- Mestel L., 1963, MNRAS, 126, 553
- Michael D. H., 1954, Mathematika, 1, 45
- Moffatt H., 1978, Field Generation in Electrically Conducting Fluids. Cambridge University Press, Cambridge
- Ogilvie G. I., 1998, MNRAS, 297, 291
- Ogilvie G. I., Pringle J. E., 1996, MNRAS, 279, 152
- Parrish I. J., Stone J. M., 2007, ApJ, 664, 135
- Pessah M. E., Chan C., 2008, ApJ, 684, 498
- Piontek R. A., Ostriker E. C., 2005, ApJ, 629, 849
- Quataert E., 2008, ApJ, 673, 758
- Quataert E., Dorland W., Hammett G. W., 2002, ApJ, 577, 524
- Rayleigh L., 1916, Proc. Royal Soc. A, 93, 148
- Regev O., Umurhan O. M., 2008, A&A, 481, 21
- Rosin M., Schekochihin A., Rincon F., Cowley S., 2011, MNRAS, 413, 7
- Rubin V. C., Ford Jr. W. K., 1970, ApJ, 159, 379
- Schekochihin A. A., Cowley S. C., 2006, Physics of Plasmas, 13, 056501
- Schekochihin A. A., Cowley S. C., Kulsrud R. M., Hammett G. W., Sharma P., 2005, ApJ, 629, 139
- Schekochihin A. A., Cowley S. C., Rincon F., Rosin M. S., 2010, MNRAS, 405, 484
- Sellwood J. A., Balbus S. A., 1999, ApJ, 511, 660
- Shakura N. I., Sunyaev R. A., 1973, A&A, 24, 337
- Sharma P., Hammett G. W., Quataert E., 2003, ApJ, 596, 1121
- Sharma P., Hammett G. W., Quataert E., Stone J. M., 2006, ApJ, 637, 952
- Sharma P., Quataert E., Hammett G. W., Stone J. M., 2007, ApJ, 667, 714
- Skinner M. A., Ostriker E. C., 2010, ApJ, 188, 290
- Sofue Y., Rubin V., 2001, ARA&A, 39, 137
- Spitzer L., 1962, Physics of Fully Ionized Gases. Interscience, New York
- Stone J., Gardiner T., Teuben P., Hawley J., Simon J., 2008, Astrophysical Journal Supplement, 178, 137
- Tamburro D., Rix H., Leroy A. K., Low M., Walter F., Kennicutt R. C., Brinks E., de Blok W. J. G., 2009, ApJ, 137, 4424
- Umurhan O. M., Regev O., 2004, A&A, 427, 855
- Velikhov E. P., 1959, JETP, 36, 1398
- Wang P., Abel T., 2009, ApJ, 696, 96
- Watson G. N., 1944, A Treatise on the Theory of Bessel Functions, second edn. Cambridge University Press, Cambridge

APPENDIX A: LINEAR STABILITY ANALYSIS

The linearised equations (1) to (4) are, in component form,

$$\gamma \delta u_r - 2 \frac{\delta u_\phi}{r} = -\frac{d\delta\Pi}{dr} + i\sigma\delta B_r - 2\frac{B\cos\theta\delta B_\phi}{r} - \frac{d\delta Z}{dr} - 3\frac{\cos^2\theta}{r}\delta Z, \quad (\text{A1})$$

$$\gamma \delta u_\phi + \frac{\delta u_r}{r} = \frac{B\cos\theta\delta B_r}{r} + i\sigma\delta B_\phi + 3ik\frac{\sin 2\theta}{2}\delta Z, \quad (\text{A2})$$

$$\gamma \delta u_z = -ik\delta\Pi + i\sigma\delta B_z - ik(1 - 3\sin^2\theta)\delta Z, \quad (\text{A3})$$

$$\gamma \delta B_r = i\sigma\delta u_r, \quad (\text{A4})$$

$$\gamma \delta B_\phi = i\sigma\delta u_\phi - \frac{\delta B_r}{r} + \frac{B\cos\theta\delta u_r}{r}, \quad (\text{A5})$$

$$\gamma \delta B_z = i\sigma\delta u_z, \quad (\text{A6})$$

$$ik\delta u_z = -\frac{1}{r}\frac{d(r\delta u_r)}{dr}, \quad (\text{A7})$$

$$\delta Z = \frac{S_B}{3}B^2\left[\left(\cos^2\theta - i\frac{k\sin 2\theta}{\gamma}\right)\frac{\delta u_r}{r} + ik\sin^2\theta\delta u_z + ik\frac{\sin 2\theta}{2}\delta u_\phi\right], \quad (\text{A8})$$

where $Z = S_B B^2 \mathbf{bb} : \nabla \mathbf{u}$. Equations (A1)-(A8) form a closed set which we can combine into a single differential equation. Eliminating the perturbed magnetic fields, stress, pressure and the vertical component of the velocity field yields two coupled ordinary differential equations for δu_r and δu_ϕ

$$C_0 \frac{d\delta u_\phi}{dr} + C_1 \delta u_\phi = C_2 \frac{d^2\delta u_r}{dr^2} + C_3 \frac{d\delta u_r}{dr} + C_4 \delta u_r, \quad (\text{A9})$$

$$D_0 \delta u_\phi = D_1 \frac{d\delta u_r}{dr} + D_2 \delta u_r, \quad (\text{A10})$$

where

$$C_0 = \frac{1}{r}k^2 2 \left(1 - i\frac{\sigma}{\gamma}B\cos\theta\right) - ikS_B\sigma^2\cos^2\theta\cot\theta, \quad (\text{A11})$$

$$C_1 = -ikS_B\sigma^2\frac{\sin^2\theta}{2}, \quad (\text{A12})$$

$$C_2 = -\gamma^{-1}(\gamma^2 + \sigma^2) - S_B\sigma^2\sin^2\theta, \quad (\text{A13})$$

$$C_3 = \frac{1}{r}\left[-\frac{1}{\gamma}(\gamma^2 + \sigma^2) + S_B\sigma^2(E_0 - \cot^2\theta)\right], \quad (\text{A14})$$

$$C_4 = \frac{1}{\gamma}(\gamma^2 + \sigma^2)\left(k^2 + \frac{1}{r^2}\right) + \frac{1}{r^2}\left[\frac{2k^2}{\gamma}B\cos\theta\left(B\cos\theta - i\frac{\sigma}{\gamma}\right) + S_B\sigma^2E_0(\cot^2\theta - 1)\right], \quad (\text{A15})$$

$$D_0 = \gamma^2 + \sigma^2 + \gamma S_B\sigma^2\cos^2\theta, \quad (\text{A16})$$

$$D_1 = -ik^{-1}S_B\gamma\sigma^2\cos\theta\sin\theta, \quad (\text{A17})$$

$$D_2 = \frac{1}{r}\left[\sigma\left(2iB\cos\theta + \frac{\sigma}{\gamma} - \frac{\gamma}{\sigma}\right) + \frac{i}{k}S_B\gamma\sigma^2\cot\theta E_0\right], \quad (\text{A18})$$

$$E_0 = -ik\gamma^{-1}\sin\theta\cos\theta + \cos^2\theta - \sin^2\theta. \quad (\text{A19})$$

Equations (A9) and (A10) can then readily be combined into equation (6). Solutions to this equation are modified Bessel functions and so the functional forms of the perturbed fields are:

$$\delta u_r = K_{iv_n}(pr)\exp[ikz + \gamma t], \quad (\text{A20})$$

$$\delta u_\phi = \frac{D_1}{D_0}\frac{d\delta u_r}{dr} + \frac{D_2}{D_0}\delta u_r, \quad (\text{A21})$$

$$\delta u_z = \frac{i}{k}\frac{1}{r}\frac{d(r\delta u_r)}{dr}, \quad (\text{A22})$$

$$\delta B_r = i\frac{\sigma}{\gamma}\delta u_r, \quad (\text{A23})$$

$$\delta B_\phi = i\frac{\sigma}{\gamma}\frac{D_1}{D_0}\frac{d\delta u_r}{dr} + \left[i\frac{\sigma}{\gamma}\frac{D_2}{D_0} + \frac{1}{r}\left(\frac{B\cos\theta}{\gamma} - i\frac{\sigma}{\gamma^2}\right)\right]\delta u_r, \quad (\text{A24})$$

$$\delta B_z = -\frac{\sigma}{\gamma}\frac{1}{kr}\frac{d(r\delta u_r)}{dr}, \quad (\text{A25})$$

$$\delta\Pi = \frac{(\gamma^2 + \sigma^2)}{k^2\gamma}\frac{1}{r}\frac{d(r\delta u_r)}{dr} - S_BB^2\left(\frac{1}{3} - \sin^2\theta\right)\left[\left(\frac{D_2}{D_0} - \sin^2\theta\right)\frac{d\delta u_r}{dr} + \left(\frac{E_0}{r} + ik\frac{\sin 2\theta}{2}\frac{D_1}{D_0}\right)\delta u_r\right]. \quad (\text{A26})$$